Dalton Transactions

RSC Publishing

PAPER

View Article Online
View Journal | View Issue

Published on 19 July 2013. Downloaded by Pennsylvania State University on 02/01/2014 19:49:37.

Cite this: *Dalton Trans.*, 2013, **42**, 14021

Synthesis, photophysics, and reverse saturable absorption of platinum complexes bearing extended π-conjugated C^N^N ligands†

Zhongjing Li and Wenfang Sun*

The synthesis of ligands **1-L–6-L** that feature the 6-[9,9-di(2-ethylhexyl)-7-*R*-9*H*-fluoren-2-yl]-2,2′-bipyridine (C^N^N) core (*R* = 4-R′-phenylethynyl with R′ = NO_2, benzothiazol-2-yl (BTZ), H and OCH_3 or *R* = 4′-BTZ-phenyl or BTZ) and their platinum complexes **1–6** were reported in this paper. The photophysical properties of these ligands and the Pt(II) complexes, including the UV-vis absorption spectra, emission characteristics at room temperature and at 77 K, and the triplet transient difference absorption spectra, were systematically investigated in order to understand the effects of the substituent at the 4-position of the 1-ethynylphenyl component and the extension of π-conjugation between the C^N^N core and the BTZ substituent. Reverse saturable absorption (RSA) of complexes **1–6** was demonstrated at 532 nm using 4.1 ns laser pulses. The UV-vis absorption spectra of **1-L–6-L** are featured by strong $^1\pi,\pi^*$ transitions in the blue spectral region, and the absorption bands are effectively red-shifted by substitution at the 4-position of the ethynylphenyl motif and by the extended π-conjugation of the linkage. A similar effect was observed for the fluorescence spectra of these ligands in CH_2Cl_2 at room temperature, but the nature of the fluorescence varies from $^1\pi,\pi^*$ fluorescence in **3-L** and **6-L**, to intraligand charge transfer (^{1}ILCT) fluorescence in **1-L**, **2-L** and **5-L**; while **4-L** possesses mixed $^1\pi,\pi^*/^1$ILCT characters. All ligands exhibit moderate triplet transient absorption (TA) in the visible spectral region, with substitution at the 4-position of the ethynylphenyl component broadening of the TA bands, while extended π-conjugation of the linkage inducing red-shifts of the TA bands. For Pt(II) complexes **1–6**, their UV-vis absorption spectra constitute red-shifted $^1\pi,\pi^*$ transitions and low-energy metal-to-ligand charge transfer (^{1}MLCT/^{1}ILCT) tails. The emission of these complexes at room temperature in CH_2Cl_2 predominantly originates from the C^N^N core localized $^3\pi,\pi^*$ state, probably mixed with minor ^{3}MLCT character. 4-Position substitution and extended π-conjugation on the ligands exert a negligible effect on the shape and energy of the emission spectra. Similar to their respective ligands, **1–6** all exhibit broader and red-shifted TA spectra with respect to their ligands and both the 4-position substitution and extended π-conjugation bathochromically shift the TA band maxima. The nonlinear transmission experiments carried out for **1–6** at 532 nm reveal that all complexes exhibit strong reverse saturable absorption (RSA), and the degree of RSA follows this trend: **6** <**4** <**5** <**2** ≤**3** <**1**. The RSA performance is efficiently improved by electron-withdrawing substituents (NO_2 and BTZ) and by extending the π-conjugation; while electron-donating substituent (OCH_3 in **4**) decreases the RSA at 532 nm.

Received 1st June 2013,
Accepted 17th July 2013

DOI: 10.1039/c3dt51430g

www.rsc.org/dalton

Introduction

Square-planar platinum(II) complexes have gained intense interest in the past two decades due to their potential applications as antitumor reagents,[1–4] in organic light emitting diodes (OLED),[5–7] photon upconversion,[8–10] and as nonlinear absorbing materials,[11–14] *etc.* Most of these applications are intrigued by their rich photophysical properties that are closely associated with their long-lived triplet excited states due to the heavy-atom enhanced spin–orbit coupling. It has been reported that the photophysical properties of the Pt(II)

Department of Chemistry and Biochemistry, North Dakota State University, Fargo, ND 58108-6050, USA. E-mail: wenfang.sun@ndsu.edu; Fax: +1 701 231 8831; Tel: +1 701 231 6254

†Electronic supplementary information (ESI) available: The synthetic procedures and ^{1}H NMR data of **6**, **7b**, and **9**, the absorption and emission spectra of **1-L**, **4-L–6-L** and **1–6** in different solvents, the emission spectra at different concentrations in CH_2Cl_2 and Stern–Volmer plots of **1**, **2**, **4–6**, the nanosecond time-resolved transient difference absorption spectra of **2-L–6-L** and **2–6**, and the emission quantum yields of **1-L–6-L** and **1–6** in different solvents. See DOI: 10.1039/c3dt51430g

This journal is © The Royal Society of Chemistry 2013

Published on 19 July 2013. Downloaded by Pennsylvania State University on 02/01/2014 19:49:37.

complexes can be readily tuned by structural modifications of the ligands. Therefore, understanding the structure–property correlations is critical for designing platinum complexes with a predetermined application. It is found that variation of substituent on the ligand from electron-withdrawing to electron-donating groups,[15] tuning the degree of π-conjugation in the ligand,[16] alternation of different linkages between components in ligand,[17] and changing configuration of the Pt(II) complexes (*cis* or *trans*)[18] could all influence the photophysics of the platinum complexes.

Our group has extensively studied the photophysics and nonlinear absorption of platinum complexes bearing polypyridine ligands (terpyridine or diimine) or cyclometalating C^N^N ligands.[11–14] Most of the complexes exhibited excellent reverse saturable absorption (RSA, *i.e.* an increase of absorptivity of molecules with the increased incident energy, and consequently a decrease of transmission with increased incident energy) for 532 nm ns laser pulses, which is typically related to the large ratios of the excited-state absorption cross section to that of the ground state of the molecule. Studies by our group on platinum bipyridine bisacetylide complexes[14] revealed that the triplet excited states and RSA can be efficiently tuned by the auxiliary substituent on the acetylide ligands. Recently, we studied the effects of the substituent at the cyclometalating C^N^N ligand on the photophysics and RSA of a series of Pt(II) complexes and discovered that the electron-donating or withdrawing substituents can significantly influence the excited-state characteristics and RSA.[19] Our studies on Pt(II) bipyridine acetylide complexes discovered that extending the π-conjugation on the bipyridine or/and the acetylide ligands can significantly increase the triplet excited-state lifetime and dramatically improve the RSA at 532 nm for ns laser pulses.[20] Intrigued by these studies, we wonder if the extended π-conjugation on the cyclometalating C^N^N ligand could also prolong the triplet excited-state lifetime and enhance the RSA of the Pt(II) complexes; and whether the terminal substituent at the extended π-conjugated C^N^N ligand would influence the photophysics and RSA of the complexes.

To answer these questions, five Pt(II) complexes containing a 6-[9,9-di(2-ethylhexyl)-7-*R*-fluoren-2-yl]-2,2′-bipyridine ligand or a 6-[9,9-di(2-ethylhexyl)-7-(4-(benzothiazol-2-yl)phenyl)-fluoren-2-yl]-2,2′-bipyridine ligand (complexes **1–5** in Scheme 1) were synthesized and their photophysics and RSA were systematically investigated. For comparison of the effect of extended π-conjugation, complex **6** that was reported previously[19] was also included in this paper. In complexes **1–4**, different substituents were introduced at the 4-position of the ethynylphenyl unit. In complexes **2**, **5**, and **6**, the linkage between the C^N^N core and the benzothiazol-2-yl (BTZ) component was varied from single bond (**6**) to phenyl (**5**) to ethynylphenyl (**2**). Comparison of the photophysics and RSA of **1–4** would allow the terminal substituent effect to be evaluated; while investigation of **2**, **5** and **6** would help us to better understand the linkage effect and thus the extended π-conjugation effect.

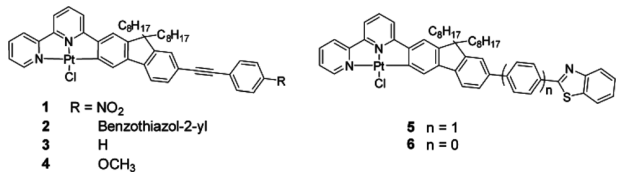

Scheme 1 Structures for complexes **1–6** (C_8H_{17} = 2-ethylhexyl).

Experimental section

Synthesis and characterization

The synthetic routes for ligands **1-L–5-L** and complexes **1–5** are illustrated in Scheme 2. The synthesis of ligand **6-L** and complex **6** has been reported previously.[19] 1-Ethynyl-4-nitrobenzene (**7a**), phenylacetylene (**7c**), and 1-ethynyl-4-methoxybenzene (**7d**) were purchased from Aldrich Co. All of the other reagents and solvents were purchased from Aldrich Chemical Co. or Alfa Aesar and used as is unless otherwise stated. Silica gel for column chromatography was purchased from Sorbent Technology (60 Å, 230–400 mesh, 500–600 m^2 g^{-1}, pH: 6.5–7.5). The synthesis of precursors **8**[21] and **11**[22] followed the literature procedures. The synthesis and characterization of precursors **6**, **7b**, and **9** were described in the ESI.† The synthetic procedures and characterization data for the key precursors **10a–10d**, **12**, ligands **1-L–5-L** and complexes **1–5** are provided below. Sonogashira coupling reactions between **7a–7d** and **9** respectively yielded **10a–10d**. Suzuki coupling reaction between **6** and **11** formed compound **12**. **10a–10d** and **12** then reacted with **8** respectively under Suzuki coupling reaction conditions to afford **1-L–5-L**. The ligands **1-L–5-L** reacted respectively with K_2PtCl_4 in refluxing acetic acid under argon for 24 hours to afford complexes **1–5**. All intermediates,

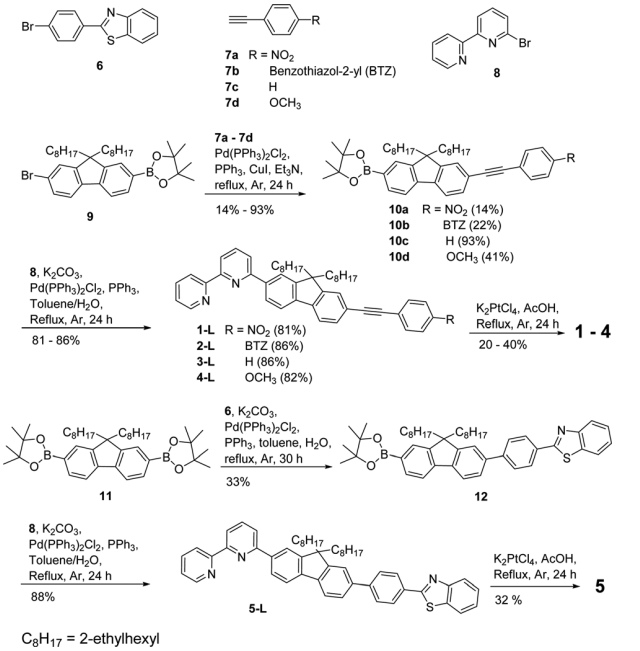

Scheme 2 Synthetic routes for ligands **1-L–5-L** and complexes **1–5**.

 This journal is © The Royal Society of Chemistry 2013

Published on 19 July 2013. Downloaded by Pennsylvania State University on 02/01/2014 19:49:37.

ligands and the Pt(II) complexes were characterized by ^{1}H NMR. Ligands **1-L–5-L** and complexes **1–5** were also characterized by electrospray ionization high-resolution mass spectrometry (ESI-HRMS), and elemental analyses.

^{1}H NMR spectra were obtained on Varian Oxford-VNMR spectrometers (300 MHz, 400 MHz, or 500 MHz). ESI-HRMS analyses were performed on a Bruker BioTOF III mass spectrometer. Elemental analyses were conducted by NuMega Resonance Laboratories, Inc. in San Diego, California.

General synthetic procedure for 10a–10d

The mixture of **7a–7d** (1.0 mmol), **9** (0.94 mmol), CuI (40 mg), $Pd(PPh_3)_2Cl_2$ (40 mg), PPh_3 (80 mg), and Et_3N (20 mL) was heated to reflux under argon for 24 hours. After reaction, the solid was removed by filtration and Et_3N was removed by distillation. Purification was carried out by column chromatography (silica gel) eluted with mixed solvent of hexane and dichloromethane (v/v = 2/1 for **10a** and **10b**; v/v = 5/1 for **10c** and **10d**).

10a. 90 mg yellow oil was collected as the product (yield: 14%). ^{1}H NMR ($CDCl_3$, 500 MHz): 8.19–8.22 (m, 2H), 7.77–7.84 (m, 2H), 7.64–7.71 (m, 4H), 7.49–7.55 (m, 2H), 1.93–2.06 (m, 4H), 1.34 (m, 12H), 0.45–0.95 (m, 30H).

10b. 0.16 g light yellow oil was collected as the product (yield: 22%). ^{1}H NMR ($CDCl_3$, 500 MHz): 8.09–8.12 (m, 3H), 7.93–7.94 (d, J = 8.0 Hz, 1H), 7.81–7.88 (m, 2H), 7.68–7.73 (m, 5H), 7.51–7.60 (m, 3H), 7.36–7.43 (m, 3H), 1.97–2.10 (m, 4H), 1.39 (s, 12H), 0.50–0.99 (m, 30H).

10c. 0.54 g light yellow oil was collected as the product (yield: 93%). ^{1}H NMR ($CDCl_3$, 400 MHz): 7.80–7.87 (m, 2H), 7.68–7.70 (d, J = 11.2 Hz, 2H), 7.50–7.59 (m, 3H), 7.29–7.38 (m, 10H), 1.95–2.08 (m, 4H), 1.37 (s, 11H), 0.49–0.94 (m, 30H).

10d. 0.25 g light yellow oil was collected as the product (yield: 41%). ^{1}H NMR ($CDCl_3$, 400 MHz): 7.77–7.83 (m, 2H), 7.65–7.67 (m, 2H), 7.45–7.51 (m, 4H), 6.86–6.88 (m, 2H), 3.82 (s, 3H), 1.93–2.05 (m, 4H), 1.35 (s, 12H), 0.46–0.92 (m, 30H).

Synthesis of 12

The mixture of **6** (0.3 g, 1 mmol), **11** (0.65 g, 1 mmol), K_2CO_3 (0.52 g), $Pd(PPh_3)_2Cl_2$ (48 mg), PPh_3 (78 mg), toluene (15 mL), and water (10 mL) was heated to reflux under argon for 30 hours. After reaction, the solid was removed by filtration and the organic phase was washed with brine and dried over $MgSO_4$. After removal of the solvent, the residue was purified by running a silica gel column eluted with a mixed solvent of dichloromethane and hexane (v/v = 1/3). 0.24 g colorless oil was collected as the product (yield: 33%). ^{1}H NMR ($CDCl_3$, 500 MHz): 8.21 (d, J = 8.0 Hz, 1H), 8.12 (d, J = 8.0 Hz, 1H), 7.94 (d, J = 8.0 Hz, 1H), 7.89 (d, J = 9.0 Hz, 1H), 7.81–7.84 (m, 2H), 7.78 (d, J = 8.0 Hz, 2H), 7.74 (d, J = 7.5 Hz, 1H), 7.67 (m, 1H), 7.63–7.65 (m, 1H), 7.52 (t, J = 7.5 Hz, 1H), 7.41 (t, J = 7.8 Hz, 1H), 2.05–2.14 (m, 4H), 1.39 (s, 12H), 0.52–0.91 (m, 30H).

General synthetic procedure for 1-L–5-L

The mixture of **8** (0.20 mmol), **10a–10d** or **12** (0.18 mmol), K_2CO_3 (0.60 g), $Pd(PPh_3)_2Cl_2$ (40 mg), PPh_3 (60 mg), toluene (10 mL), and water (5 mL) was heated to reflux under argon for 24 hours. After reaction, the solid was removed by filtration and the organic phase was collected and washed with brine and dried over $MgSO_4$. After removal of the solvent, the residue was purified by running a silica gel column eluted with dichloromethane.

1-L. 0.10 g yellow oil was collected as the product (yield: 81%). ^{1}H NMR ($CDCl_3$, 400 MHz): 8.68–8.69 (m, 1H), 8.64 (d, J = 7.6 Hz, 1H), 8.37 (d, J = 7.6 Hz, 1H), 8.20–8.22 (m, 2H), 8.12–8.17 (m, 2H), 7.78–7.90 (m, 4H), 7.74 (d, J = 7.6 Hz, 1H), 7.65–7.69 (m, 2H), 7.57–7.60 (m, 1H), 7.54–7.56 (m, 1H), 7.30–7.33 (m, 1H), 2.00–2.16 (m, 4H), 0.51–0.95 (m, 30H). Elemental analysis calculated for $C_{47}H_{51}N_3O_2{\cdot}0.125CH_2Cl_2{\cdot}0.25C_6H_{14}$: C, 80.88; H, 7.64; N, 5.82. Found: C, 81.27; H, 8.07; N, 5.80. ESI-HRMS: m/z calc. for $[C_{47}H_{51}N_3O_2 + H]^+$: 690.4054; Found: 690.4035.

2-L. 0.12 g yellow solid was collected as the product (yield: 86%). ^{1}H NMR ($CDCl_3$, 400 MHz): 8.68–8.70 (m, 1H), 8.64–8.66 (m, 1H), 8.35–8.38 (m, 1H), 8.11–8.17 (m, 1H), 8.06–8.10 (m, 3H), 7.77–7.91 (m, 5H), 7.72–7.74 (d, J = 8.0 Hz, 1H), 7.64–7.69 (m, 2H), 7.58–7.60 (m, 1H), 7.54–7.57 (m, 1H), 7.47–7.51 (m, 1H), 7.36–7.40 (m, 1H), 7.28–7.33 (m, 2H), 2.01–2.16 (m, 4H), 0.52–0.97 (m, 30H). Elemental analysis calculated for $C_{54}H_{55}N_3S{\cdot}0.25CH_2Cl_2$: C, 81.52; H, 7.00; N, 5.26. Found: C, 81.12; H, 7.35; N, 5.37. ESI-HRMS: m/z calc. for $[C_{54}H_{55}N_3S + H]^+$: 778.4189; Found: 778.4162.

3-L. 0.10 g yellow oil was collected as the product (yield: 86%). ^{1}H NMR ($CDCl_3$, 400 MHz): 8.65–8.71 (m, 2H), 8.37–8.39 (m, 1H), 8.12–8.18 (m, 2H), 7.71–7.91 (m, 5H), 7.52–7.57 (m, 4H), 7.31–7.38 (m, 4H), 2.01–2.17 (m, 4H), 0.50–0.95 (m, 30H). Elemental analysis calculated for $C_{47}H_{52}N_2{\cdot}0.1CH_2Cl_2$: C, 86.58; H, 8.05; N, 4.29. Found: C, 86.89; H, 8.37; N, 4.30. ESI-HRMS: m/z calc. for $[C_{47}H_{52}N_2 + H]^+$: 645.4203; Found: 645.4172.

4-L. 0.10 g yellow oil was collected as the product (yield: 82%). ^{1}H NMR ($CDCl_3$, 400 MHz): 8.65–8.71 (m, 2H), 8.36–8.38 (m, 1H), 8.11–8.18 (m, 2H), 7.83–7.91 (m, 2H), 7.79–7.81 (m, 2H), 7.70–7.71 (m, 1H), 7.48–7.56 (m, 4H), 7.31–7.34 (m, 1H), 6.88–6.90 (m, 2H), 3.83 (s, 3H), 2.00–2.16 (m, 4H), 0.52–0.97 (m, 30H). Elemental analysis calculated for $C_{48}H_{54}N_2O{\cdot}0.25CH_2Cl_2{\cdot}0.25C_6H_{14}$: C, 83.25; H, 8.15; N, 3.90. Found: C, 83.21; H, 8.43; N, 4.02. ESI-HRMS: m/z calc. for $[C_{48}H_{54}N_2O + H]^+$: 675.4309; Found: 675.4283.

5-L. 0.12 g yellow solid was collected as the product (yield: 88%). ^{1}H NMR ($CDCl_3$, 400 MHz): 8.66–8.70 (m, 2H), 8.36–8.38 (m, 1H), 8.13–8.20 (m, 4H), 8.09 (d, J = 8.4 Hz, 1H), 7.75–7.91 (m, 8H), 7.68 (m, 1H), 7.62–7.65 (dt, J = 8.0, 1.6 Hz, 1H), 7.47–7.51 (m, 1H), 7.36–7.40 (m, 1H), 7.30–7.33 (m, 1H), 2.07–2.21 (m, 4H), 0.51–0.92 (m, 30H). Elemental analysis calculated for $C_{52}H_{55}N_3S$: C, 82.82; H, 7.35; N, 5.57. Found: C, 82.42; H, 7.44; N, 5.52. ESI-HRMS: m/z calc. for $[C_{52}H_{55}N_3S + H]^+$: 754.4189; Found: 754.4167.

General synthetic procedure for 1–5

The mixture of **1-L–5-L** (0.17 mmol), K_2PtCl_4 (72 mg, 0.17 mmol), and acetic acid (10 mL) was refluxed under argon for 24 hours. After reaction, the solvent was removed by

Published on 19 July 2013. Downloaded by Pennsylvania State University on 02/01/2014 19:49:37.

distillation. The red solid was purified by column chromatography on silica gel eluted with dichloromethane. Further purification was carried out by recrystallization from dichloromethane and hexane.

1. 62 mg red powder was collected as the product (yield: 40%). ^{1}H NMR ($CDCl_3$, 400 MHz): 8.93–9.00 (m, 1H), 8.19–8.22 (m, 2H), 8.11–8.12 (m, 1H), 7.90–7.95 (m, 2H), 7.81–7.84 (m, 1H), 7.72–7.79 (m, 1H), 7.64–7.69 (m, 2H), 7.46–7.54 (m, 5H), 7.30–7.31 (m, 1H), 1.94–2.03 (m, 4H), 0.48–0.94 (m, 30H). Elemental analysis calculated for $C_{47}H_{50}ClN_3O_2Pt$: C, 61.40; H, 5.48; N, 4.57. Found: C, 61.34; H, 5.72; N, 4.51. ESI-HRMS: *m*/*z* calc. for $[C_{47}H_{50}N_3O_2PtCl + H]^+$: 920.3317; Found: 920.3355.

2. 52 mg yellow powder was collected as the product (yield: 30%). ^{1}H NMR ($CDCl_3$, 400 MHz): 9.17–9.19 (m, 1H), 8.14 (s, 1H), 8.04–8.09 (m, 4H), 7.89–7.92 (m, 2H), 7.81–7.83 (m, 2H), 7.64–7.66 (m, 3H), 7.47–7.56 (m, 5H), 7.36–7.40 (m, 1H), 7.33 (m, 1H), 1.98–1.99 (m, 4H), 0.48–0.92 (m, 30H). Elemental analysis calculated for $C_{54}H_{54}ClN_3PtS{\cdot}0.5CH_2Cl_2$: C, 62.34; H, 5.28; N, 4.00. Found: C, 62.48; H, 5.54; N, 4.00. ESI-HRMS: *m*/*z* calc. for $[C_{54}H_{54}N_3SPtCl + H]^+$: 1008.3453; Found: 1008.3501.

3. 30 mg yellow powder was obtained as the product (yield: 20%). ^{1}H NMR ($CDCl_3$, 500 MHz): 9.04–9.08 (m, 1H), 8.14 (s, 1H), 7.93–8.01 (m, 2H), 7.77–7.84 (m, 2H), 7.52–7.58 (m, 7H), 7.33–7.39 (m, 4H), 1.97–2.05 (m, 4H), 0.52–0.96 (m, 30H). Elemental analysis calculated for $C_{47}H_{51}ClN_2Pt$: C, 64.56; H, 5.88; N, 3.20. Found: C, 64.10; H, 6.21; N, 3.13. ESI-HRMS: *m*/*z* calc. for $[C_{47}H_{51}N_2PtCl + H]^+$: 875.3466; Found: 875.3432.

4. 46 mg yellow powder was obtained as the product (yield: 30%). ^{1}H NMR ($CDCl_3$, 400 MHz): 9.08–9.11 (m, 3H), 8.10 (s, 1H), 7.96–7.99 (m, 1H), 7.90 (d, J = 8.0 Hz, 1H), 7.75–7.80 (m, 2H), 7.45–7.59 (m, 7H), 7.29 (d, J = 1.6 Hz, 1H), 6.85–6.87 (m, 2H), 3.81 (s, 3H), 1.96–1.97 (m, 4H), 0.47–0.94 (m, 30H). Elemental analysis calculated for $C_{48}H_{53}ClN_2OPt$: C, 63.74; H, 5.91; N, 3.10. Found: C, 63.55; H, 5.91; N, 3.05. ESI-HRMS: *m*/*z* calc. for $[C_{48}H_{53}N_2OPtCl + H]^+$: 905.3572; Found: 905.3592.

5. 53 mg yellow powder was obtained as the product (yield: 32%). ^{1}H NMR ($CDCl_3$, 400 MHz): 9.24–9.26 (m, 1H), 8.19–8.21 (m, 3H), 8.08–8.11 (m, 2H), 7.92–7.94 (m, 3H), 7.83–7.86 (m, 1H), 7.78–7.80 (m, 2H), 7.65–7.67 (m, 2H), 7.49–7.60 (m, 6), 7.38–7.42 (m, 2H), 2.00–2.10 (m, 4H), 0.49–0.94 (m, 30H). Elemental analysis calculated for $C_{52}H_{54}ClN_3PtS{\cdot}0.33CH_2Cl_2$: C, 62.12; H, 5.45; N, 4.15. Found: C, 61.86; H, 5.49; N, 4.14. ESI-HRMS: *m*/*z* calc. for $[C_{52}H_{54}N_3SPtCl + H]^+$: 984.3452; Found: 984.3462.

Photophysical measurements

The spectroscopic grade solvents used for the photophysical experiments were purchased from VWR International and used as is without further purification. A Shimadzu UV-2501 spectrophotometer was used to record the UV-vis absorption spectra in different solvents. A SPEX fluorolog-3 fluorometer/phosphorometer was used to measure the steady-state emission spectra. The emission spectra of **1–6** were recorded after their solutions were purged with argon for 30 minutes. The emission quantum yields of **1-L–6-L** and **1–6** were determined by the relative actinometry method[23] (**1–6** were measured in degassed solutions). A degassed aqueous solution of $[Ru(bpy)_3]Cl_2$ (Φ_{em} = 0.042, λ_{ex} = 436 nm)[24] was used as the reference for complexes **1–6**, and a 1 N sulfuric acid solution of quinine bisulfate (Φ_{em} = 0.546, λ_{ex} = 347.5 nm)[25] was used as the reference for ligands **1-L–6-L**.

The nanosecond transient difference absorption (TA) spectra and decays of **1-L–6-L** and **1–6** were measured in degassed CH_3CN solutions on an Edinburgh LP920 laser flash photolysis spectrometer. The third harmonic output (355 nm) of a Nd:YAG laser (Quantel Brilliant, pulse width: 4.1 ns, repetition rate was set at 1 Hz) was used as the excitation source. Each sample was purged with argon for 30 min prior to measurement. The triplet excited-state absorption coefficient (ε_T) at the TA band maximum was determined by the singlet depletion method.[26] The triplet quantum yields (Φ_T) of **1–6** were determined by the relative actinometry using SiNc in benzene as the reference (ε_{590} = 70 000 M^{-1} cm^{-1}, Φ_T = 0.20).[27]

Nonlinear transmission experiment

The reverse saturable absorption of complexes **1–6** was characterized by nonlinear transmission experiment at 532 nm using a Quantel Brilliant laser as the light source. The pulse width of the laser was 4.1 ns and the repetition rate was set at 10 Hz. The complexes were dissolved in CH_2Cl_2. The concentration of the sample solution was adjusted to obtain a linear transmission of 90% at 532 nm in a 2 mm-thick cuvette. The experimental setup is similar to that reported previously,[28] with a 40 cm plano-convex lens being used to focus the beam to the center of the 2 mm-thick sample cuvette. The radius of the beam waist at the focal point was approximately 96 μm.

Results and discussion

Electronic absorption

The electronic absorption of **1-L–6-L** and **1–6** were measured in dichloromethane in the concentration range of 1×10^{-6}–1×10^{-4} mol L^{-1}, and the spectra are shown in Fig. 1a for the

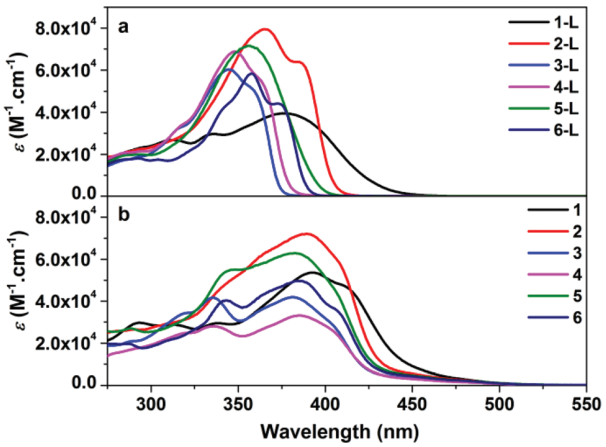

Fig. 1 (a) UV-vis absorption spectra of ligands **1-L–6-L** measured in CH_2Cl_2; (b) UV-vis absorption spectra of complexes **1–6** measured in CH_2Cl_2.

 This journal is © The Royal Society of Chemistry 2013

Published on 19 July 2013. Downloaded by Pennsylvania State University on 02/01/2014 19:49:37.

Table 1 Electronic absorption, emission (room temperature and 77 K), and excited-state absorption parameters for complexes **1–6** and ligands **1-L–6-L**

	λ_{abs}/nm (ε/L mol^{-1} cm^{-1})[a]	λ_{em}/nm (τ_0/μs; k_{sq}/L mol^{-1} s^{-1}); Φ_{em}[b] R. T.	λ_{em}/nm (τ_{em}/μs)[c] 77 K	$\lambda_{T_1-T_n}$/nm (τ_T/μs; $\varepsilon_{T_1-T_n}$/L mol^{-1} cm^{-1}; Φ_T)[d]
1	450 (9120), 410 (47 670), 393 (53 650), 338 (29 500)	593 (7.5; 1.53 × 10^9), 638 (7.0; 1.60 × 10^9); 0.13	583 (26.1), 632 (23.9)	560 (5.1; 26 530; 0.37)
2	450 (5490), 410 (55 380), 389 (72 130), 366 (63 380)	592 (6.2; 1.63 × 10^9), 636 (6.2; 1.26 × 10^9); 0.053	585 (26.1), 633 (28.1)	675 (8.1; 90 010; 0.19)
3	450 (3270), 405 (28 100), 381 (41 910), 336 (41 630)	589 (4.7; 1.66 × 10^9), 630 (4.5; 1.21 × 10^9); 0.084	577 (22.4), 626 (20.9)	610 (5.7; 37 510; 0.43)
4	450 (3030), 400 (28 300), 385 (33 170), 335 (27 980)	591 (4.6; 1.69 × 10^9), 635 (4.5; 1.31 × 10^9); 0.051	578 (22.9), 627 (23.3)	640 (7.1; 37 190; 0.25)
5	450 (4650), 405 (46 110), 382 (62 880), 348 (55 090)	590 (3.4; 1.79 × 10^9), 640 (3.4; 1.26 × 10^9); 0.069	576 (24.7), 623 (23.0)	650 (7.3; 60 730; 0.12)
6	450 (4310), 404 (37 320), 385 (49 820), 343 (40 510)	588 (6.1; 1.44 × 10^9), 634 (6.1; 9.33 × 10^8); 0.092	581 (24.0), 630 (28.0)	625 (8.2; 56 980; 0.33)
1-L	400 (29 080), 377 (39 530)	571 (–); 0.032	485	510 (26.7; –; –)
2-L	384 (63 900), 366 (79 400)	428 (–); 0.92	430, 461	625 (12.3; –; –)
3-L	357 (52 000), 344 (60 230)	393 (–); 0.96	378, 392, 413	555 (14.0; –; –)
4-L	363 (55 150), 348 (68 850)	400 (–); 0.99	383, 399, 416	530 (29.6; –; –)
5-L	371 (56 100), 356 (71 580)	427 (–); 0.92	402, 421, 462	610 (15.3; –; –)
6-L	373 (44 200), 358 (58 250)	410 (–); 0.80	395, 410, 437	580 (24.0; –; –)

[a] Absorption band maximum (λ_{abs}) and molar extinction coefficient (ε_{max}) in CH_2Cl_2. [b] Emission wavelength (λ_{em}), intrinsic lifetime (τ_0), self-quenching rate constant (k_{sq}), and emission quantum yield measured in CH_2Cl_2 with $Ru(bpy)_3Cl_2$ as the standard for the complexes and quinine bisulfate for the ligands. [c] In BuCN glassy matrix. [d] Triplet excited-state absorption band maximum ($\lambda_{T_1-T_n}$), molar extinction coefficient ($\varepsilon_{T_1-T_n}$), quantum yield (Φ_T) and lifetime (τ_T) measured in CH_3CN.

ligands and Fig. 1b for the complexes. The absorption band maxima and molar extinction coefficients for the ligands and the complexes are summarized in Table 1. No ground-state aggregation was evident in the concentration range studied, as supported by the obedience of the absorption to the Beer's law. The major absorption bands of **1-L–6-L** appear at the 300 nm–450 nm region with the molar extinction coefficients being in the order of 10^4 L mol^{-1} cm^{-1}. Considering the large molar extinction coefficients and the minor solvent effect (see Fig. S1–S6 of the ESI†), these bands are ascribed to the $^1\pi,\pi^*$ transitions. The UV-vis absorption spectra of the Pt(II) complexes **1–6** are featured by strong absorption bands below *ca.* 430 nm (450 nm for **1**) and a broad tail from 440 nm (450 nm for **1**) to 500 nm. Comparing to the UV-vis absorption spectra of their respective ligands and with reference to the other Pt(II) C^N^N chloride complexes with similar structures,[29] the major absorption bands can be attributed to predominantly the ligand centered $^1\pi,\pi^*$ transitions; while the broad tail is believed to be dominated by the ^{1}MLCT transition, probably mixed with some intraligand charge transfer (from the ethynylfluorene component to the bipyridine component) characters. The $^1\pi,\pi^*$ transitions in the complexes are significantly red-shifted compared to those in their respective ligands, indicating the electron delocalization induced by the interactions with the metal ion.

Comparing the UV-vis absorption spectra of **1-L–4-L**, it is very clear that substitution at the 4-position of the ethynylphenyl (regardless electron-donating or electron-withdrawing substituent) causes pronounced red-shifts of the absorption bands and/or increased molar extinction coefficients, as evidenced by **1-L**, **2-L** and **4-L** compared to **3-L**, which suggests electron delocalization induced by the substituents. Notably, the absorption spectrum of **1-L** is much broader and red-shifted, but with significantly low molar extinction coefficients with respect to the other ligands. This implies that there could be strong mixing of the intramolecular charge transfer character with the $^1\pi,\pi^*$ transition in **1-L**, which decreases the $^1\pi,\pi^*$ transition oscillation strength but increases the intramolecular charge transfer transition oscillation strength. In contrast, the absorption of **2-L–4-L** should be dominated by the $^1\pi,\pi^*$ transitions. Comparison of the UV-vis absorption spectra of **2-L**, **5-L** and **6-L** reveals that with the extended π-conjugation between the BTZ unit and the C^N^N core, the UV-vis absorption spectra of **2-L** and **5-L** are pronouncedly red-shifted and their molar extinction coefficients are dramatically increased.

Although the effects of terminal substituent and linkage variation on the $^1\pi,\pi^*$ transitions are significant for the ligands, these effects become much weaker in complexes **1–6**. The ligand centered $^1\pi,\pi^*$ transitions of complexes **3–6** are essentially at the same energy except for that they are obviously red-shifted in **1** and **2**. However, the molar extinction coefficient still increases with the terminal substitution and extended π-linkage except for **4**. In contrast, the effect of the π-linkage on the charge-transfer tails of **2**, **5** and **6** is more pronounced. The tail in **2** and **5** are clearly more red-shifted and stronger than that in **6**.

Photoluminescence

The emission spectra of **1-L–6-L** and **1–6** in dichloromethane at room temperature and in butyronitrile glassy matrix at 77 K were measured and shown in Fig. 2. The emission band maxima, lifetimes and quantum yields for the ligands and complexes are summarized in Table 1.

As shown in Fig. 2a, the emission of the ligands **3-L** and **6-L** in CH_2Cl_2 is featured by distinct vibronic structures, while the emission from **4-L** is slightly structured. In contrast, the emission from **1-L**, **2-L** and **5-L** is broad and structureless. The

Published on 19 July 2013. Downloaded by Pennsylvania State University on 02/01/2014 19:49:37.

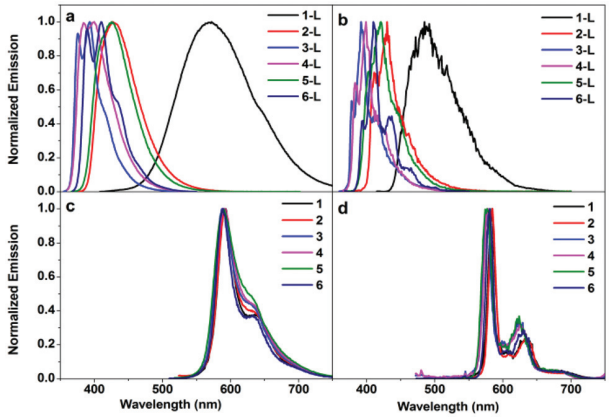

Fig. 2 (a) Normalized emission spectra of ligands **1-L–6-L** (λ_{ex} = 398 nm for **1-L**, 365 nm for **2-L**, 345 nm for **3-L**, 350 nm for **4-L**, 356 nm for **5-L**, and 358 nm for **6-L**; $c = 4 \times 10^{-5}$ mol L^{-1} for **1-L** and **3-L**, 5×10^{-6} mol L^{-1} for **2-L**, **5-L**, and **6-L**, and 1×10^{-6} mol L^{-1} for **4-L**). (b) Normalized emission spectra of **1-L–6-L** at 77 K in glassy BuCN matrix at the concentration of 1×10^{-5} mol L^{-1} (λ_{ex} = 398 nm for **1-L**, 365 nm for **2-L**, 345 nm for **3-L**, 350 nm for **4-L**, 356 nm for **5-L**, and 358 nm for **6-L**). (c) Normalized emission spectra of complexes **1–6** (λ_{ex} = 393 nm for **1**, 383 nm for **2**, 381 nm for **3**, 385 nm for **4**, 383 nm for **5**, and 383 nm for **6**) at the concentration of 2×10^{-5} mol L^{-1}. (d) Normalized emission spectra of complexes **1–6** at 77 K in glassy BuCN matrix, $c = 2 \times 10^{-5}$ mol L^{-1} (λ_{ex} = 393 nm for **1**, 383 nm for **2**, 381 nm for **3**, 385 nm for **4**, 383 nm for **5**, and 383 nm for **6**).

lifetimes of the emission from the ligands are too short to be measured on our spectrometer. This suggests that the emission of the ligands predominantly originates from the $^1\pi,\pi^*$ state for **3-L** and **6-L**, but predominantly emanates from the ^{1}ILCT (intraligand or intramolecular charge transfer state) for **1-L**, **2-L** and **5-L** in CH_2Cl_2. For **4-L**, the emission exhibits mixed characters of $^1\pi,\pi^*/^1$ILCT. This assignment is supported by the different solvatochromic effects for these ligands. As demonstrated in Fig. 3 for **2-L** and **3-L** and in ESI Fig. S13–S16† for the other four ligands, **3-L** and **6-L** exhibit minor solvatochromic effects, with the similar shape of spectra in both polar and nonpolar solvents and a slight red-shift when the polarity of solvent increases. These features are characteristics of $^1\pi,\pi^*$ fluorescence. However, for the other four ligands, the fluorescence spectra become structureless and drastically red-shifted in polar solvents (such as CH_2Cl_2 and CH_3CN), reflecting the transition from $^1\pi,\pi^*$ character in less polar solvents to ^{1}ILCT character in more polar solvents. Comparing the emission spectra of **1-L–6-L**, it is clear that the fluorescence energy

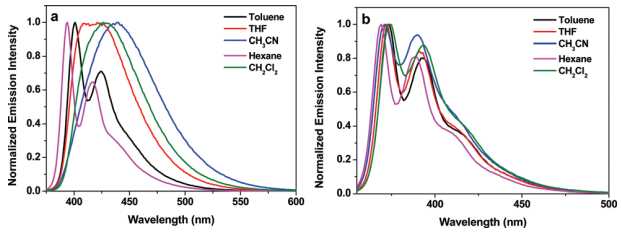

Fig. 3 Normalized emission spectra of (a) **2-L** and (b) **3-L** in different solvents. λ_{ex} = 347.5 nm.

trend follows the similar trend as the UV-vis absorptions, namely, both substitution and extended π-conjugation of the linkage between the BTZ substituent and the C^N^N core effectively lower the fluorescence energy. In addition, both the substitution and extended π-conjugation lead to significant charge transfer characters in their respective fluorescence spectra in polar solvents. It is worth noting that the strong electron withdrawing group like NO_2 in **1-L** plays the most significant role in switching the emission into charge transfer fluorescence, testified by the solvatochromic study shown in Fig. S13,† in which the emission was only observed in dichloromethane and THF but diminished in nonpolar solvents such as hexane and toluene and in the more polar solvent CH_3CN.

The emission spectra of **1-L–6-L** in butyronitrile glassy matrix at 77 K are shown in Fig. 2b. The spectra become narrower and more structured (except **1-L**) in comparison to those at room temperature but essentially remain of similar energy. Therefore, they are attributed to the low-temperature fluorescence.

The emission spectra of the Pt(II) complexes **1–6** in CH_2Cl_2 at room temperature are displayed in Fig. 2c. Despite the different substituents and π-linkage, the emission spectra of these complexes all resemble each other, with a remarkable Stokes shift, distinct vibronic structure, long lifetime (3.4–7.5 μs), and minor solvatochromic effect (see Fig. S17–S22 of ESI†). Taking these features into account, we can assign the observed emission of **1–6** to the phosphorescence predominantly from the C^N^N core localized $^3\pi,\pi^*$ state. However, contribution from the ^{3}MLCT state is possible in view of the several microsecond lifetime, which is relatively shorter than a pure $^3\pi,\pi^*$ phosphorescence, and the minor but clear negative solvatochromic effect. This assignment is also supported by the small thermally induced Stokes shifts for these complexes, *i.e.* 289 cm^{-1} for **1**, 202 cm^{-1} for **2**, 353 cm^{-1} for **3**, 381 cm^{-1} for **4**, 412 cm^{-1} for **5**, and 205 cm^{-1} for **6**. This phenomenon is also consistent with that observed from the Pt(II) complexes with a 2-(9,9-dihexadecyl-7-(4-*R*-phenylethynyl)-fluoren-2-yl)-1,10-phenanthroline ligand.[29]

A concentration-dependent emission study of **1–6** in CH_2Cl_2 was conducted. As exemplified in Fig. 4 for complex **3**, the emission intensity increases with increased concentration up to 2×10^{-5} mol L^{-1}. Above this concentration, the emission intensity decreases when the concentration gets higher. Considering the remarkable ground-state absorption of this complex at the excitation wavelength (381 nm), the primary inner-filter effect is clearly a cause. Contribution from the ground-state aggregation can be excluded because our concentration-dependent UV-vis absorption study described earlier confirms that no ground-state aggregation occurs in the concentration range used in our study. However, lifetime measurements reveal that the lifetime of the solution keeps decreasing with increased concentration, which clearly indicates the presence of self-quenching. The self-quenching rate constant deduced for **3** at 589 nm emission wavelength is 1.66×10^9 L mol^{-1} s^{-1}, which is in line with those reported for Pt(II) terpyridine, Pt(C^N^N) or Pt(II) diimine complexes.[16,30] Similar

 This journal is © The Royal Society of Chemistry 2013

Published on 19 July 2013. Downloaded by Pennsylvania State University on 02/01/2014 19:49:37.

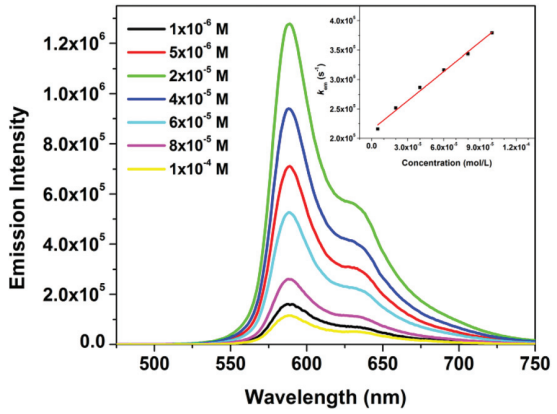

Fig. 4 Concentration-dependent emission spectra of complex **3** in CH_2Cl_2. λ_{ex} = 381 nm. The inset shows the Stern–Volmer plot monitored at 589 nm.

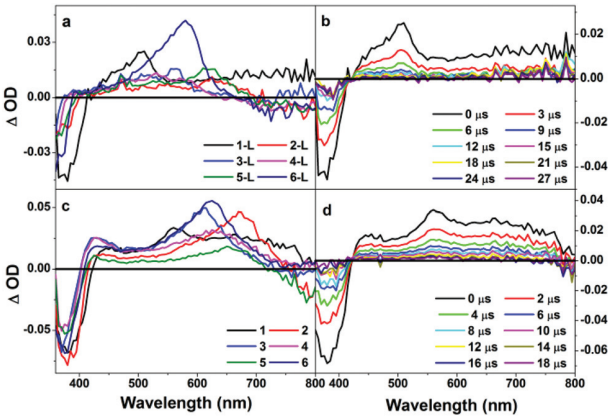

Fig. 5 Nanosecond transient difference absorption spectra of (a) ligands **1-L–6-L** at zero delay after excitation; (b) time-resolved TA spectra of **1-L**; (c) complexes **1–6** at zero delay after excitation; (d) time-resolved TA spectra of **1**. All of the spectra were measured in CH_3CN, λ_{ex} = 355 nm, A_{355} = 0.4 in a 1 cm cuvette.

phenomena were observed from the other five complexes, and the results are provided in the ESI Fig. S23–S28† and in Table 1.

The emission spectra of **1–6** at 77 K BuCN glassy matrix are presented in Fig. 2d. These spectra are somewhat blue-shifted and become more structured and narrower with respect to those at room temperature, which are ascribed to the rigidochromic effect.[31] The vibronic progressions for **1–6** are in the range of 1212–1357 cm^{-1}, and the thermally induced Stokes shifts for these complexes are approximately 200–410 cm^{-1}. All these features indicate the $^3\pi,\pi^*$ nature of the emission at 77 K for these complexes.

Transient absorption

The nanosecond transient difference absorption (TA) measurements were conducted for ligands **1-L–6-L** and complexes **1–6** in acetonitrile to understand the triplet excited-state characteristics. By performing the transient absorption experiments, the spectral feature of the triplet excited-state absorption can be obtained, and the spectral region where the excited state absorbs stronger than the ground state can be identified from the positive absorption band(s) of the TA spectrum. In addition, the excited-state lifetime and the triplet excited-state quantum yield can be deduced from the decay of the TA and determined by the relative actinometry, respectively.

The nanosecond transient absorption spectra of **1-L–6-L** at zero delay after excitation are displayed in Fig. 5a. In addition to the bleaching bands in the UV region that correspond to the ground-state absorption bands, all the ligands show moderate to strong transient absorption in the visible spectral region. Compared to **3-L**, the TA bands of **1-L**, **2-L** and **4-L** are much broader. For the three ligands with different π-conjugated linkages, *i.e.* **2-L**, **5-L**, and **6-L**, the major TA band is noticeably red-shifted from **6-L**, to **5-L**, and to **2-L** although the TA bands of **2-L** and **5-L** are weaker. The TAs of all of the ligands show well time-resolved decay as illustrated for **1-L** in Fig. 5b and in Fig. S29–S33† for **2-L–6-L**. The lifetimes deduced from the decay of TA are all tens of μs, implying that the excited state giving rise to the observed TA spectra should be the $^3\pi,\pi^*$.

The TA spectra of **1–6** at zero delay after excitation are illustrated in Fig. 5c. The triplet excited-state lifetimes, extinction coefficients, and quantum yields are deduced or calculated and the results are summarized in Table 1. The TA spectra of all complexes possess three characteristic bands: the bleaching band in the blue spectral region corresponding to their respective $^1\pi,\pi^*$ absorption band, the moderate and narrow TA band in the wavelength range of 400–500 nm, and the broad and strong TA band in the wavelength range of 500–700 nm. The energy of the 500–700 nm TA band varies with the terminal substituent and the extent of π-conjugation between the C^N^N core and the BTZ unit: both electron-withdrawing and electron-donating substituents (NO_2 in **1**, BTZ in **2**, and OCH_3 in **4**) cause a red-shift of the major TA band, extending the π-conjugation in the linkage also effectively red-shifts the major TA bands in **2** and **5** compared to that in **6**. From the decay of the TA, the triplet lifetimes were deduced to be 5–8 μs, suggesting that the TA spectra likely arise from the ligand based $^3\pi,\pi^*$ state as well, which is supported by the red-shift of the major TA bands in **1–6** compared to the TA bands in their corresponding ligands. The red-shift reflects the interactions between the ligand π orbital and the metal d orbital.

Reverse saturable absorption (RSA)

As manifested by the positive absorption bands in the visible spectral region of the TA spectra, complexes **1–6** all exhibit stronger excited-state absorption than that of the ground state at 532 nm. Meanwhile, the triplet-state lifetimes are significantly longer than the ns laser pulse width (4.1 ns). Therefore, it is expected that these complexes would exhibit reverse saturable absorption (decrease of transmission with increased incident energy) for ns laser pulses at 532 nm. To verify this assumption, nonlinear transmission experiment was carried out for complexes **1–6** in CH_2Cl_2 solutions at a linear transmittance of 90% in a 2 mm cuvette using the 532 nm ns laser pulses. Fig. 6 displays the nonlinear transmission results. The

Published on 19 July 2013. Downloaded by Pennsylvania State University on 02/01/2014 19:49:37.

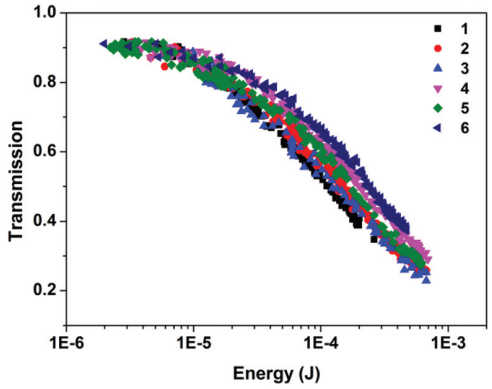

Fig. 6 Nonlinear transmission curves for **1–6** at 532 nm for 4.1 ns laser pulses. The radius of the beam waist at the focal point was approximately 96 μm. The linear transmission for all sample solutions was adjusted to 90% in a 2 mm cuvette.

Table 2 Ground-state (σ_0) and excited-state (σ_{ex}) absorption cross-sections of complexes **1–6** at 532 nm in CH_3CN

	1	**2**	**3**	**4**	**5**	**6**
$\sigma_0/10^{-18}$ cm	0.35	0.59	0.38	0.57	0.57	0.67
$\sigma_{ex}/10^{-18}$ cm	65	84	59	74	80	80
σ_{ex}/σ_0	186	142	155	130	140	125

transmissions of all of the complexes decrease remarkably with increased incident energy, which clearly demonstrates a strong RSA from these complexes. The strength of the RSA follows this trend: **6** <**4** <**5** <**2** ≤**3** <**1**. It appears that electron-withdrawing substituents (NO_2 and BTZ) enhance the RSA of **1** and **2**, while electron-donating substituent (OCH_3 in **4**) decreases the RSA at 532 nm. Extending the π-conjugation of the linkage also results in improved RSA, as evident by the trend of **6** <**5** <**2**.

To rationalize the trend of RSA performance for these complexes, the ratios of the excited-state absorption cross section with respect to that of the ground state (σ_{ex}/σ_0) at 532 nm, which is the key parameter determining the RSA, have to be evaluated. According to the ground-state absorption at 532 nm and at the wavelength of the TA band maximum, the optical density changes (ΔOD) at 532 nm and at the TA band maximum, the molar extinction coefficient at the TA band maximum ($\varepsilon_{T_1-T_n}$), and the method described by our group previously,[20b] the excited-state absorption cross sections (σ_{ex}) for **1–6** at 532 nm were estimated and the results are shown in Table 2. The calculated ratios of σ_{ex}/σ_0 follow this trend: **6** <**4** <**5** <**2** <**3** <**1**, which matches the observed RSA trend very well.

Conclusions

We have synthesized and characterized five new 6-[9,9-di-(2-ethylhexyl)-7-*R*-9*H*-fluoren-2-yl]-2,2′-bipyridine ligands (**1-L–5-L**) and their Pt(II) complexes (**1–5**) (*R* = 4-R′-phenylethynyl with R′ = NO_2, BTZ, H and OCH_3 or *R* = 4′-BTZ-phen-1-yl). The ligand **6-L** and its Pt(II) complex reported earlier were also included in this paper for comparison purpose. The effects of terminal substituents and the different π-conjugated linkages between the BTZ component and the C^N^N core on the photophysics of these ligands and complexes and on the RSA of the complexes were systematically investigated. It is found that both the terminal substitution and extended π-conjugation of the linkage cause pronounced red-shift of the UV-vis absorption bands and the fluorescence bands in the ligands; and induces significant intraligand charge transfer character in their fluorescence in polar solvents like CH_2Cl_2 and CH_3CN. **1-L–6-L** all exhibit moderate triplet transient absorption in the visible spectral region. Terminal substitution causes a broadening of the TA bands in **1-L**, **2-L** and **4-L**; while extended π-conjugation in the linkage induces a red-shift of the TA bands in **2-L** and **5-L** compared to that in **6-L**. After complexation with the Pt(II) ion, the major absorption bands in the formed complexes **1–6** all bathochromically shift compared to those of their respective ligands, accompanied by a low-energy charge transfer tail. Terminal substitution and extending π-conjugation exert similar effects to those observed in the ligands. In contrast, the emission spectra and energies are essentially independent of the variation of the substituent and degree of π-conjugation for **1–6**, suggesting a C^N^N core localized $^3\pi,\pi^*$ phosphorescence in nature. Similar to the trend observed in the UV-vis absorption spectra, the TA bands in **1–6** also red-shift with terminal substitution and extended π-conjugation. These bands also notably shift to lower energy compared to those in their corresponding ligands. The ground-state absorption and transient absorption studies demonstrate that the absorption properties of both the ground state and the excited state can be efficiently tuned by structural modifications. As a result, complexes **1–6** exhibit strong RSA for ns laser pulses at 532 nm. The degree of RSA (**6** <**4** <**5** <**2** ≤**3** <**1**) is also affected by the substituents and the π-conjugation on the ligand. The RSA performance is efficiently improved by electron-withdrawing substituents (NO_2 and BTZ) and by extending the π-conjugation; while electron-donating substituent (OCH_3 in **4**) decreases the RSA at 532 nm. The broadband excited-state absorption, long triplet lifetime and strong RSA of **1–6** at 532 nm suggest these complexes could be promising nonlinear absorbing materials for photonic device applications.

Acknowledgements

This work is partially supported by the National Science Foundation (CAREER CHE-0449598) and partially by the Army Research Laboratory (W911NF-06-2-0032 and W911NF-10-2-0055) to W. Sun.

Notes and references

1 B. Rosenberg, L. VanCamp, J. E. Trosko and V. H. Mansour, *Nature*, 1969, **222**, 385.

 This journal is © The Royal Society of Chemistry 2013

Published on 19 July 2013. Downloaded by Pennsylvania State University on 02/01/2014 19:49:37.

2 S. Piccinonna, N. Margiotta, C. Pacifico, A. Lopalco, N. Denora, S. Fedi, M. Corsini and G. Natile, *Dalton Trans.*, 2012, **41**, 9689.
3 B. Chiavarino, M. E. Crestoni, S. Fornarini, D. Scuderi and J.-Y. Salpin, *J. Am. Chem. Soc.*, 2013, **135**, 1445.
4 S. Chen, D. Xu, H. Jiang, Z. Xi, P. Zhu and Y. Liu, *Angew. Chem., Int. Ed.*, 2012, **51**, 12258.
5 L. Xiao, Z. Chen, B. Qu, J. Luo, S. Kong, Q. Gong and J. Kido, *Adv. Mater.*, 2011, **23**, 926.
6 J. R. Sommer, A. H. Shelton, A. Parthasarathy, I. Ghiviriga, J. R. Reynolds and K. S. Schanze, *Chem. Mater.*, 2011, **23**, 5296.
7 Y. Wu, S.-X. Wu, H.-B. Li, Y. Geng and Z.-M. Su, *Dalton Trans.*, 2011, **40**, 4480.
8 P. Du and R. Eisenberg, *Chem. Sci.*, 2010, **1**, 502.
9 Y. Liu, W. Wu, J. Zhao, X. Zhang and H. Guo, *Dalton Trans.*, 2011, **40**, 9085.
10 T. N. Singh-Rachford, A. Haefele, R. Ziessel and F. N. Castellano, *J. Am. Chem. Soc.*, 2008, **130**, 16164.
11 R. Vestberg, R. Westlund, A. Eriksson, C. Lopes, M. Carlsson, B. Eliasson, E. Glimsdal, M. Lindgren and E. Malmström, *Macromolecules*, 2006, **39**, 2238.
12 W. Sun, B. Zhang, Y. Li, T. M. Pritchett, Z. Li and J. E. Haley, *Chem. Mater.*, 2010, **22**, 6384.
13 B. Zhang, Y. Li, R. Liu, T. M. Pritchett, A. Azenkeng, A. Ugrinov, J. E. Haley, Z. Li, M. R. Hoffmann and W. Sun, *Chem.–Eur. J.*, 2012, **18**, 4593.
14 (*a*) Z. Li, E. Badaeva, D. Zhou, J. Bjorgaard, K. D. Glusac, S. Killina and W. Sun, *J. Phys. Chem. A*, 2012, **116**, 4878; (*b*) R. Liu, D. Zhou, A. Azenkeng, Z. Li, Y. Li, K. D. Glusac and W. Sun, *Chem.–Eur. J.*, 2012, **18**, 11440.
15 M. Hissler, W. B. Connick, D. K. Geiger, J. E. McGarrah, D. Lipa, R. J. Lachicotte and R. Eisenberg, *Inorg. Chem.*, 2000, **39**, 447.
16 X.-G. Liu and W. Sun, *Inorg. Chim. Acta*, 2012, **388**, 140.
17 Z. Ji, S. Li, Y. Li and W. Sun, *Inorg. Chem.*, 2010, **49**, 1337.
18 K. Haskins-Glusac, I. Ghiviriga, K. A. Abboud and K. S. Schanze, *J. Phys. Chem. B*, 2004, **108**, 4969.
19 Z. Li, E. Badaeva, A. Ugrinov, S. Kilina and W. Sun, *Inorg. Chem.*, 2013, **52**, 7578.
20 (*a*) R. Liu, A. Azenkeng, D. Zhou, Y. Li, K. D. Glusac and W. Sun, *J. Phys. Chem. A*, 2013, **117**, 1907; (*b*) Y. Li, R. Liu, E. Badaeva, S. Kilina and W. Sun, *J. Phys. Chem. C*, 2013, **117**, 5908.
21 D. Shin and C. Switzer, *Chem. Commun.*, 2007, 4401.
22 Y. Geng, S. W. Culligan, A. Trajkovska, J. U. Wallace and S. H. Chen, *Chem. Mater.*, 2003, **15**, 542.
23 J. N. Demas and G. A. Crosby, *J. Phys. Chem.*, 1971, **75**, 991.
24 J. Van Houten and R. Watts, *J. Am. Chem. Soc.*, 1976, **98**, 4853.
25 D. F. Eaton, *Pure Appl. Chem.*, 1988, **60**, 1107.
26 I. Carmichael and G. L. Hug, *J. Phys. Chem. Ref. Data*, 1986, **15**, 1.
27 P. A. Firey, W. E. Ford, J. R. Sounik, M. E. Kenney and M. A. J. Rodgers, *J. Am. Chem. Soc.*, 1988, **110**, 7626.
28 F. Guo, W. Sun, Y. Liu and K. Schanze, *Inorg. Chem.*, 2005, **44**, 4055.
29 X.-G. Liu and W. Sun, *Eur. J. Inorg. Chem.*, 2013, DOI: 10.1002/ejic.201300466.
30 (*a*) P. Shao, Y. Li, T. M. Pritchett and W. Sun, *Inorg. Chem.*, 2010, **49**, 4507; (*b*) Z. Ji, A. Azenkeng, M. Hoffmann and W. Sun, *Dalton Trans.*, 2009, 7725.
31 S. Lai, M. C. W. Chan, K. Cheung and C. Che, *Inorg. Chem.*, 1999, **38**, 4262.